

Research Paper

Temperature Influence on Non-Linear Harmonic Vibrations of Plates Made of Viscoelastic Materials

Przemysław LITEWKA*, Roman LEWANDOWSKI

*Institute of Structural Analysis
Poznan University of Technology*

Piotrowo 5, 60-965 Poznań, Poland

e-mail: roman.lewandowski@put.poznan.pl

*Corresponding Author e-mail: przemyslaw.litewka@gmail.com

This paper is devoted to the analysis of ambient temperature influence on harmonic vibrations of von Kármán geometrically non-linear plates. The time-temperature superposition and the Williams-Landel-Ferry formula for the horizontal shift are used to modify the viscosity properties in the fractional Zener material model of viscoelasticity. The non-linear amplitude equation is obtained from the time-averaged principle of virtual work and the harmonic balance method. It is then solved after the finite element (FE) discretization using the continuation method to get the response curves in the frequency domain. Several numerical examples are solved and a significant influence of temperature on the resonance properties of the analysed plates is observed.

Key words: von Kármán plates; fractional Zener material; harmonic vibrations; time-temperature superposition.

1. INTRODUCTION

Plates are one of the most important structural elements, used very widely in engineering. As the entire structures or as fragments thereof, they are subjected to various types of external influences, among them – dynamic excitation. Thus, in many cases, plates are undergoing vibrations and the question of their reduction may become important in many engineering applications.

There are numerous ways to reduce vibrations, and one of them is the use of viscoelastic (VE) materials that exhibit damping properties. These materials can be implemented as layers, patches, etc., and in some cases, the complete plates may be made of VE material. It is also known that even the traditional structural materials like wood, RC concrete, fibre-reinforced concrete, etc., possess some viscoelastic properties. In this situation the elaboration of models capable of describing the VE plates is vital. There exist numerous papers presenting results

of analyses of VE plates. The summary of those works can be found in [3]. In the analyses various models of VE were taken into account. For instance, classical Zener [5] and Kelvin models were used in [15], where natural vibrations of thick VE plates on VE foundations were considered. The hereditary integral description was applied in [26] to get some results for the problem of plate vibrations. Free vibrations of circular and annular plates with the first-order shear deformation theory and Zener material model were considered in [1] and analytical solutions for some particular cases were given.

The stability of non-linear vibrations of VE plates with the VE model using the Boltzman hereditary principle was investigated in [10, 25].

AMABILI [4] analysed non-linear forced vibrations of plates with the Kelvin VE model and viscous damping. Also, the cases with geometric imperfections were considered. Free vibrations of VE plates with the fractional Kelvin model were considered in [20].

Circular plates with viscoelasticity modelled with the hereditary Boltzmann law, as well as the first and higher-order shear deformation, were solved analytically in [23].

Results of experimental testing were published, too. In [2] forced vibrations of VE thin rectangular plates with the standard linear solid material model taking into account the relation between the retardation time and the vibration mode were considered. A very good match between the experimental measurements for the steel plate and the numerical results was found. Vibrations of plates with plant-reinforcing fibres were analysed and tested experimentally in [11].

It is a known fact that the damping properties of many VE materials, especially polymers, depend significantly on the temperature [8, 24]. Thus in the present paper, a continuation of the authors' earlier work [16, 17] on forced vibrations of VE plates with classical and fractional Zener material is presented. The common approach to the problem of temperature influence is the use of the time-temperature superposition rule [8, 24], where the assessment of the shift parameters using the Williams-Landel-Ferry formula is presented. This proposal is limited to rheologically simple materials. In the following, we also assume that the thermal state of the plate is steady. Furthermore, the result from [12, 13] will be used, where the analysis of frames with VE dampers indicated that it is only necessary to introduce the temperature modification of the viscosity parameter in Zener material. The details of the VE model with temperature influence are given in Sec. 2. In Sec. 3, the von Kármán formulation for the plate with the first-order shear deformation theory is presented. Section 4 summarises the main steps of the derivation of amplitude equation, which are given in detail in [12]. In Sec. 5, information on the FE discretization is included. A few numerical examples of plate vibrations in different temperature conditions are solved in Sec. 6. Finally, concluding remarks are formulated in Sec. 7.

2. FRACTIONAL ZENER MATERIAL MODEL WITH TEMPERATURE INFLUENCE

The introduction of fractional derivatives [22] to replace the classical ones with the integer order in the modelling of viscoelasticity dates back to works by BAGLEY and TORVIK [6, 7]. Since that time, this concept has been successfully applied to generalise the classical VE models [4, 9, 18], and to their specific application to plates as well, as indicated in Sec. 1. It is commonly recognised that the use of fractional derivatives allows to describe the behaviour of many VE materials with a relatively small number of material parameters, when compared to the classical formulations. In the present formulation, the Zener material model with fractional derivative is used. The general relation between strain ε and stress σ takes the form:

$$(2.1) \quad \sigma + \tau_M D_t^\alpha \sigma = E_1 \varepsilon + \tau_M E_\infty D_t^\alpha \varepsilon,$$

where the fractional derivative with respect to time in the Riemann-Liouville version is used

$$(2.2) \quad D_t^\alpha f(t) = \frac{1}{\Gamma(1-\alpha)} \frac{d}{dt} \int_a^t \frac{f(\tau)}{(t-\tau)^\alpha} d\tau$$

and the relaxed and non-relaxed moduli are denoted by E_1 and E_∞ . The relaxation time is defined as t_M . The schematic representation of the model is shown in Fig. 1, and it includes two springs with the stiffness parameters E_K and E_M as well as a Scott-Blair fractional damping element characterised by the damping parameter c and the order of the fractional derivative α . The relations between the parameters in (2.1) and in Fig. 1 take the form

$$(2.3) \quad E_1 = E_K, \quad E_\infty = E_K + E_M, \quad \tau_M = \frac{c}{E_M}.$$

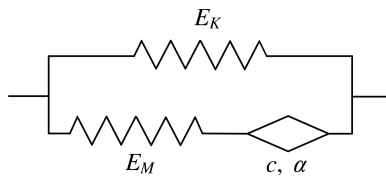


FIG. 1. Fractional Zener material model.

The influence of temperature on the damping properties of viscoelastic materials is frequently described with the use of the time-temperature superposition. This rule, valid for so-called rheologically simple materials, with numerous polymers belonging to this group, states that the difference between the modulus-frequency curves for the reference temperature T_0 and the current temperature T

is not in their shape but lies in shifting, only. Furthermore, for the majority of the considered materials, only a horizontal shifting (in the direction of frequency) is important [8]. This horizontal shift, denoted by a_T , can be obtained by several methods. Among them, the most frequently recognised method is based on the Williams-Landel-Ferry formula taking the form

$$(2.4) \quad \log a_T = \frac{-C_1 (T - T_0)}{C_2 + T - T_0},$$

where C_1 and C_2 are the material parameters that have to be determined experimentally.

In the present formulation, one more important result reported in [12, 13] is used, too. In [12, 13], it was shown that while analysing the structural elements made of various VE materials, obtaining the temperature-influenced dynamic characteristics is possible when only the damping property of the material model is modified by the shift (2.4). The spring parameters remain unchanged. So, in the following, it will be assumed that the temperature-affected damping parameter c_T of the fractional Zener material will replace its reference value c , according to the formula

$$(2.5) \quad c_T = a_T c,$$

leading to a similar modification of the relaxation time

$$(2.6) \quad \tau_{MT} = a_T \tau_M.$$

3. PLATE FORMULATION

The plate is modelled using the classical von Kármán geometric non-linear theory and the first-order shear deformation theory. The internal forces: bending moments M_x and M_y with the torsional moment M_{xy} , two shear forces Q_x and Q_y , as well as the in-plane forces – normal N_x and N_y and shear N_{xy} , are assembled into vectors

$$(3.1) \quad \mathbf{M} = \text{col} (M_x \ M_y \ M_{xy}),$$

$$(3.2) \quad \mathbf{Q} = \text{col} (Q_x \ Q_y),$$

$$(3.3) \quad \mathbf{N} = \text{col} (N_x \ N_y \ N_{xy}).$$

The corresponding strain measures are expressed in terms of generalised displacements of the plate mid-plane: cross-section rotations φ , deflection w^0 , and in-plane translations u^0, v^0 :

$$(3.4) \quad \boldsymbol{\varepsilon}_r = \text{col} [\varphi_{x,x} \ \varphi_{y,y} \ (\varphi_{x,y} + \varphi_{y,x})],$$

$$(3.5) \quad \boldsymbol{\varepsilon}_s = \text{col} [(w^0_{,x} + \varphi_x) \ (w^0_{,y} + \varphi_y)],$$

$$(3.6) \quad \boldsymbol{\varepsilon}_p = \boldsymbol{\varepsilon}_{pl} + \boldsymbol{\varepsilon}_{pn} = \text{col} \left[\begin{matrix} u_{,x}^0 & v_{,y}^0 & (u_{,y}^0 + v_{,x}^0) \end{matrix} \right] \\ + \text{col} \left[\begin{matrix} \frac{1}{2}(w_{,x}^0)^2 & \frac{1}{2}(w_{,y}^0)^2 & w_{,x}^0 w_{,y}^0 \end{matrix} \right],$$

where the subscripts after comma indicate the derivation with respect to the specified co-ordinate. By using the same relations between the stresses and the internal forces as in the elastic material, the physical relations between internal forces and strain measures in the isotropic fractional Zener material model can be written down in the form

$$(3.7) \quad \mathbf{M} + \tau_M D_t^\alpha \mathbf{M} = \mathbf{D}_1 \boldsymbol{\varepsilon}_r + \tau_M \mathbf{D}_\infty D_t^\alpha \boldsymbol{\varepsilon}_r,$$

$$(3.8) \quad \mathbf{Q} + \tau_M D_t^\alpha \mathbf{Q} = \mathbf{A}_{q1} \boldsymbol{\varepsilon}_s + \tau_M \mathbf{A}_{q\infty} D_t^\alpha \boldsymbol{\varepsilon}_s,$$

$$(3.9) \quad \mathbf{N} + \tau_M D_t^\alpha \mathbf{N} = \mathbf{A}_1 \boldsymbol{\varepsilon}_l + \tau_M \mathbf{A}_\infty D_t^\alpha \boldsymbol{\varepsilon}_l,$$

where the physical matrices have the form known from elasticity

$$(3.10) \quad \mathbf{D}_i = \frac{E_i h^3}{12(1-\nu^2)} \mathbf{E},$$

$$(3.11) \quad \mathbf{A}_{qi} = \frac{\kappa E_i h^2}{2(1+\nu)} \begin{bmatrix} 1 & 0 \\ 0 & 1 \end{bmatrix},$$

$$(3.12) \quad \mathbf{A}_i = \frac{E_i h}{1-\nu^2} \mathbf{E}.$$

Here $i = 1$ or ∞ , h represents the plate thickness, ν – the Poisson’s ratio and

$$\mathbf{E} = \begin{bmatrix} 1 & \nu & 0 \\ \nu & 1 & 0 \\ 0 & 0 & (1-\nu)/2 \end{bmatrix}.$$

In the following, it is assumed that the Poisson’s ratio is not changing with temperature.

4. AMPLITUDE EQUATION

In this paper, the harmonic forced vibrations of the plates are analysed. The function of excitation as a distributed transverse loading p_w is assumed to have one harmonic and two amplitudes p_{wc} , p_{ws} what leads to the expression

$$(4.1) \quad p_w = p_{wc} \cos \lambda t + p_{ws} \sin \lambda t,$$

where λ is the excitation frequency and subscripts c and s refer to the sine and cosine amplitudes.

The resulting form of the plate response in generalised displacements must be compatible with the excitation (4.1) and must fit to the plate formulation (3.4)–(3.6) where the non-linear terms are present. Thus, the predicted displacements functions, assembled into suitable vectors, read

$$(4.2) \quad \mathbf{q}_w = \{w^0\} = \mathbf{q}_{wc} \cos \lambda t + \mathbf{q}_{ws} \sin \lambda t,$$

$$(4.3) \quad \mathbf{q}_t = \left\{ \begin{array}{c} u^0 \\ v^0 \end{array} \right\} = \mathbf{q}_{tc} \cos^2 \lambda t + \mathbf{q}_{t0} \cos \lambda t \sin \lambda t + \mathbf{q}_{ts} \sin^2 \lambda t,$$

$$(4.4) \quad \mathbf{q}_r = \left\{ \begin{array}{c} \varphi_x \\ \varphi_y \end{array} \right\} = \mathbf{q}_{rc} \cos \lambda t + \mathbf{q}_{rs} \sin \lambda t,$$

where the further subscripts were introduced: w refers to the direction of the plate deflection, t – to the in-plane translations and r – to the rotational directions, whereas 0 – to the sine-cosine amplitude. As a consequence, the functions of inertia forces, including rotary inertia, resulting from Newton's law and the assumed form of the displacements, can be expressed as:

$$(4.5) \quad \mathbf{b}_w = \lambda^2 \mathbf{m}_w \mathbf{q}_{wc} \cos \lambda t + \lambda^2 \mathbf{m}_w \mathbf{q}_{ws} \sin \lambda t,$$

$$(4.6) \quad \mathbf{b}_t = 2\lambda^2 [\mathbf{m}_t(\mathbf{q}_{tc} - \mathbf{q}_{ts}) \cos^2 \lambda t \\ + 2\mathbf{m}_t \mathbf{q}_{t0} \cos \lambda t \sin \lambda t - \mathbf{m}_t(\mathbf{q}_{tc} + \mathbf{q}_{ts}) \sin^2 \lambda t],$$

$$(4.7) \quad \mathbf{b}_r = \lambda^2 \mathbf{m}_r \mathbf{q}_{rc} \cos \lambda t + \lambda^2 \mathbf{m}_r \mathbf{q}_{rs} \sin \lambda t,$$

where the following mass matrices were introduced:

$$\mathbf{m}_w = [m], \quad \mathbf{m}_t = \begin{bmatrix} m & 0 \\ 0 & m \end{bmatrix} = m\mathbf{I}, \quad \mathbf{m}_r = \frac{1}{12} \begin{bmatrix} mh^2 & 0 \\ 0 & mh^2 \end{bmatrix} = m_r \mathbf{I},$$

and $m_r = mh^2/12$, whereas m is the unit area mass of the plate and \mathbf{I} is the unit matrix.

The vectors of internal forces take the form

$$(4.8) \quad \mathbf{M} = \mathbf{M}_c \cos \lambda t + \mathbf{M}_s \sin \lambda t,$$

$$(4.9) \quad \mathbf{Q} = \mathbf{Q}_c \cos \lambda t + \mathbf{Q}_s \sin \lambda t,$$

$$(4.10) \quad \mathbf{N} = \mathbf{N}_c \cos^2 \lambda t + \mathbf{N}_0 \cos \lambda t \sin \lambda t + \mathbf{N}_s \sin^2 \lambda t,$$

which are consistent with the physical relations (3.7)–(3.9). Similarly, the corresponding strain vectors are assumed as:

$$(4.11) \quad \boldsymbol{\varepsilon}_r = \boldsymbol{\varepsilon}_{rc} \cos \lambda t + \boldsymbol{\varepsilon}_{rs} \sin \lambda t,$$

$$(4.12) \quad \boldsymbol{\varepsilon}_s = \boldsymbol{\varepsilon}_{sc} \cos \lambda t + \boldsymbol{\varepsilon}_{ss} \sin \lambda t,$$

$$(4.13) \quad \varepsilon_p = \varepsilon_{pc} \cos^2 \lambda t + \varepsilon_{p0} \cos \lambda t \sin \lambda t + \varepsilon_{ps} \sin^2 \lambda t = (\varepsilon_{plc} + \varepsilon_{pnc}) \cos^2 \lambda t \\ + (\varepsilon_{pl0} + \varepsilon_{pn0}) \cos \lambda t \sin \lambda t + (\varepsilon_{pls} + \varepsilon_{pns}) \sin^2 \lambda t,$$

where, in the latter, the split into linear and non-linear parts, denoted respectively by subscripts l and n , is introduced in correspondence to (3.6). One can write down the time-averaged principle of virtual work for the plate undergoing the assumed harmonic vibrations under the action of the excitation loading as in (4.1). We obtain

$$(4.14) \quad \frac{2}{T} \int_0^T \int_A \delta \mathbf{q}_t^T \mathbf{b}_t \, dA \, dt + \frac{2}{T} \int_0^T \int_A \delta \mathbf{q}_w^T \mathbf{b}_w \, dA \, dt \\ + \frac{2}{T} \int_0^T \int_A \delta \mathbf{q}_r^T \mathbf{b}_r \, dA \, dt + \frac{2}{T} \int_0^T \int_A \delta \mathbf{q}_w^T \mathbf{p}_w \, dA \, dt \\ = \frac{2}{T} \int_0^T \int_A \delta \varepsilon_r^T \mathbf{M} \, dA \, dt + \frac{2}{T} \int_0^T \int_A \delta \varepsilon_s^T \mathbf{Q} \, dA \, dt + \frac{2}{T} \int_0^T \int_A \delta \varepsilon_p^T \mathbf{N} \, dA \, dt,$$

where A is the area of the plate mid-plane. Substitution of the proposed form of the solution (4.2)–(4.13) and carrying out the integration with respect to time leads to the following amplitude equation:

$$(4.15) \quad \lambda^2 \left[\int_A \delta \mathbf{q}_{tc}^T \mathbf{m}_t (\mathbf{q}_{tc} - \mathbf{q}_{ts}) \, dA + \int_A \delta \mathbf{q}_{t0}^T \mathbf{m}_t \mathbf{q}_{t0} \, dA - \frac{1}{2} \int_A \delta \mathbf{q}_{ts}^T \mathbf{m}_t (\mathbf{q}_{tc} - \mathbf{q}_{ts}) \, dA \right. \\ \left. + \int_A \delta \mathbf{q}_{wc}^T \mathbf{m}_w \mathbf{q}_{wc} \, dA + \int_A \delta \mathbf{q}_{ws}^T \mathbf{m}_w \mathbf{q}_{ws} \, dA + \int_A \delta \mathbf{q}_{rc}^T \mathbf{m}_r \mathbf{q}_{rc} \, dA + \int_A \delta \mathbf{q}_{rs}^T \mathbf{m}_r \mathbf{q}_{rs} \, dA \right] \\ + \int_A \delta \mathbf{q}_{wc}^T \mathbf{p}_{wc} \, dA + \int_A \delta \mathbf{q}_{ws}^T \mathbf{p}_{ws} \, dA \\ = \int_A \delta \mathbf{q}_{rc}^T \mathbf{B}'^T_r \mathbf{M}_c \, dA + \int_A \delta \mathbf{q}_{rs}^T \mathbf{B}'^T_r \mathbf{M}_s \, dA + \int_A (\delta \mathbf{q}_{wc}^T \mathbf{B}'^T_{sw} + \delta \mathbf{q}_{rc}^T \mathbf{B}'^T_{sr}) \mathbf{Q}_c \, dA \\ + \int_A (\delta \mathbf{q}_{ws}^T \mathbf{B}'^T_{sw} + \delta \mathbf{q}_{rs}^T \mathbf{B}'^T_{sr}) \mathbf{Q}_s \, dA + \frac{3}{4} \int_A \delta \varepsilon_{pc}^T \mathbf{N}_c \, dA \\ + \frac{1}{4} \int_A \delta \varepsilon_{pc}^T \mathbf{N}_s \, dA + \frac{1}{4} \int_A \delta \varepsilon_{p0}^T \mathbf{N}_0 \, dA + \frac{1}{4} \int_A \delta \varepsilon_{ps}^T \mathbf{N}_c \, dA + \frac{3}{4} \int_A \delta \varepsilon_{pc}^T \mathbf{N}_s \, dA.$$

Matrices \mathbf{B}' assemble the appropriate differential operators and the details thereof are given in Appendix.

The amplitudes of internal forces can be expressed in terms of the amplitudes of strains (and further – displacements) applying the harmonic balance method to the physical relations (3.7)–(3.9). The method leads to three separate sets of simultaneous equations (two equations corresponding to the sine and cosine amplitudes in the cases of moments and shear forces, three equations for the sine-squared, cosine-squared and sine-cosine amplitudes in the case of in-plane forces), which can be solved – see [17] for the detailed derivation. This approach yields the following expressions for the moments and the shear forces:

$$(4.16) \quad \begin{aligned} \mathbf{M}_c &= (t_1 \mathbf{D}_1 + t_3 \mathbf{D}_\infty) \boldsymbol{\varepsilon}_{rc} + t_2 (-\mathbf{D}_1 + \mathbf{D}_\infty) \boldsymbol{\varepsilon}_{rs}, \\ \mathbf{M}_s &= t_2 (\mathbf{D}_1 - \mathbf{D}_\infty) \boldsymbol{\varepsilon}_{rc} + (t_1 \mathbf{D}_1 + t_3 \mathbf{D}_\infty) \boldsymbol{\varepsilon}_{rs}, \end{aligned}$$

$$(4.17) \quad \begin{aligned} \mathbf{Q}_c &= (t_1 \mathbf{A}_{q1} + t_3 \mathbf{A}_{q\infty}) \boldsymbol{\varepsilon}_{sc} + t_2 (-\mathbf{A}_{q1} + \mathbf{A}_{q\infty}) \boldsymbol{\varepsilon}_{ss}, \\ \mathbf{Q}_s &= t_2 (\mathbf{A}_{q1} - \mathbf{A}_{q\infty}) \boldsymbol{\varepsilon}_{sc} + (t_1 \mathbf{A}_{q1} + t_3 \mathbf{A}_{q\infty}) \boldsymbol{\varepsilon}_{ss}, \end{aligned}$$

where the parameters t_j are functions of the excitation frequency, the order of the fractional derivative and the relaxation time

$$\begin{aligned} t_1 &= \frac{1 + \tau_M^\alpha \lambda^\alpha C}{(1 + \tau_M^\alpha \lambda^\alpha C)^2 + \tau_M^{2\alpha} \lambda^{2\alpha}}, \\ t_2 &= \frac{\tau_M^\alpha \lambda^\alpha (C + \tau_M^\alpha \lambda^\alpha)}{(1 + \tau_M^\alpha \lambda^\alpha C)^2 + \tau_M^{2\alpha} \lambda^{2\alpha}}, \\ t_3 &= \frac{\tau_M^\alpha \lambda^\alpha S}{(1 + \tau_M^\alpha \lambda^\alpha C)^2 + \tau_M^{2\alpha} \lambda^{2\alpha}}, \end{aligned}$$

whereas $C = \cos \frac{\alpha\pi}{2}$, $S = \sin \frac{\alpha\pi}{2}$.

For the amplitudes of in-plane forces one obtains

$$(4.18) \quad \begin{aligned} \mathbf{N}_c &= \mathbf{A}_I \boldsymbol{\varepsilon}_{pc} + \mathbf{A}_{III} \boldsymbol{\varepsilon}_{p0} + \mathbf{A}_{IV} \boldsymbol{\varepsilon}_{ps}, \\ \mathbf{N}_0 &= 2\mathbf{A}_{III} \boldsymbol{\varepsilon}_{pc} + \mathbf{A}_{II} \boldsymbol{\varepsilon}_{p0} - 2\mathbf{A}_{III} \boldsymbol{\varepsilon}_{ps}, \\ \mathbf{N}_s &= \mathbf{A}_{IV} \boldsymbol{\varepsilon}_{pc} + \mathbf{A}_{III} \boldsymbol{\varepsilon}_{p0} + \mathbf{A}_I \boldsymbol{\varepsilon}_{ps}, \end{aligned}$$

where

$$\begin{aligned} \mathbf{A}_I &= \mathbf{A}_1 + t_4 (\mathbf{A}_\infty - \mathbf{A}_1), \\ \mathbf{A}_{II} &= \mathbf{A}_1 + 2t_4 (\mathbf{A}_\infty - \mathbf{A}_1), \\ \mathbf{A}_{III} &= -t_5 (\mathbf{A}_\infty - \mathbf{A}_1), \\ \mathbf{A}_{IV} &= -t_4 (\mathbf{A}_\infty - \mathbf{A}_1), \end{aligned}$$

and

$$t_4 = \frac{2\tau_M^\alpha \lambda^\alpha (2\tau_M^\alpha \lambda^\alpha + C)}{2 + 4 \cdot 2^\alpha \tau_M^\alpha \lambda^\alpha + 2 \cdot 2^{2\alpha} \tau_M^{2\alpha} \lambda^{2\alpha}},$$

$$t_5 = \frac{2\tau_M^\alpha \lambda^\alpha S}{2 + 4 \cdot 2^\alpha \tau_M^\alpha \lambda^\alpha + 2 \cdot 2^{2\alpha} \tau_M^{2\alpha} \lambda^{2\alpha}}.$$

5. FINITE ELEMENT DISCRETISATION

The amplitude equation obtained in Sec. 4 is discretised using the finite element method.

In the examples presented in this paper, rectangular 8-noded elements with bi-quadratic shape functions N_1 to N_8 are used. The nodal degrees of freedom in the form of displacements amplitudes for a single element e are assembled into the 12-entry vector \mathbf{q}_e , composed of the following sub-vectors: three for in-plane translations – \mathbf{q}_{tec} , \mathbf{q}_{te0} , \mathbf{q}_{tes} , each containing two amplitudes; two for deflections – \mathbf{q}_{wec} , \mathbf{q}_{wes} , each containing one amplitude and two for rotations – \mathbf{q}_{rec} , \mathbf{q}_{res} , each containing two amplitudes.

The discretisation of displacements in the element is done using the appropriate matrices of shape functions

$$(5.1) \quad \mathbf{q}_{tc} = \mathbf{N}_t \mathbf{q}_{tec}, \quad \mathbf{q}_{ts} = \mathbf{N}_t \mathbf{q}_{tes}, \quad \mathbf{q}_{t0} = \mathbf{N}_t \mathbf{q}_{te0},$$

$$(5.2) \quad \mathbf{q}_{wc} = \mathbf{N}_w \mathbf{q}_{wec}, \quad \mathbf{q}_{ws} = \mathbf{N}_w \mathbf{q}_{wes},$$

$$(5.3) \quad \mathbf{q}_{rc} = \mathbf{N}_r \mathbf{q}_{rec}, \quad \mathbf{q}_{rs} = \mathbf{N}_r \mathbf{q}_{res},$$

where

$$\mathbf{N}_w = [N_1 \ N_2 \ N_3 \ N_4 \ N_5 \ N_6 \ N_7 \ N_8],$$

$$\mathbf{N}_t = \mathbf{N}_r = [\mathbf{N}_1 \ \mathbf{N}_2 \ \mathbf{N}_3 \ \mathbf{N}_4 \ \mathbf{N}_5 \ \mathbf{N}_6 \ \mathbf{N}_7 \ \mathbf{N}_8],$$

and

$$\mathbf{N}_i = \begin{bmatrix} N_i & 0 \\ 0 & N_i \end{bmatrix}, \quad i = 1, \dots, 8.$$

The final form of the FE discretised amplitude equation for a single element reads

$$(5.4) \quad \{\delta \mathbf{q}_e\}^T (-\lambda^2) [\mathbf{M}_e] \{\mathbf{q}_e\} + \{\delta \mathbf{q}_e\}^T \{\mathbf{P}_e\} + \{\delta \mathbf{q}_e\}^T [\mathbf{K}_{el}] \{\mathbf{q}_e\} + \{\delta \mathbf{q}_e\}^T [\mathbf{K}_{en}] \{\mathbf{q}_e\} = 0,$$

where \mathbf{M}_e is the element mass matrix resulting from the inertia terms in (4.15), \mathbf{P}_e is the element loading vector and \mathbf{K}_{el} , \mathbf{K}_{en} are linear and non-linear parts, respectively, of the element stiffness contribution yielding from the influence

of internal forces on the right-hand side of (4.15), see [16, 17]. The entries in \mathbf{K}_{en} depend on displacement amplitudes and, thus, they must be consistently linearised in the numerical process of solving the global non-linear equation which is obtained from the standard assembly process for the entire plate as

$$(5.5) \quad \{\delta \mathbf{q}\}^T (-\lambda^2) [\mathbf{M}] \{\mathbf{q}\} + \{\delta \mathbf{q}\}^T \{\mathbf{P}\} + \{\delta \mathbf{q}\}^T [\mathbf{K}_l] \{\mathbf{q}\} + \{\delta \mathbf{q}\}^T [\mathbf{K}_n] \{\mathbf{q}\} = 0.$$

The solution to (5.5) is found using the continuation method what leads to the response curves showing the relation between the vibration amplitudes \mathbf{q} and the excitation frequency λ . Some examples of computations are presented in the subsequent section.

6. EXAMPLES

In this section, three examples of harmonic vibrations of simply supported square plates (see Fig. 2) made from different VE materials subjected to various temperature conditions are analysed. To this end, the authors' own computer programs were used. The response curves for the deflection amplitude

$$(6.1) \quad q_w(\lambda) = \sqrt{q_{wec}^2 + q_{wes}^2}$$

of the plate midpoint are obtained using the procedure described in Sec. 5. The plates are loaded by the harmonic excitation force in the form of the point force

$$(6.2) \quad P_w = P \cos \lambda t$$

applied at the plate midpoint. The plate is modelled by 36 finite plate elements discussed in Sec. 5, forming the regular mesh 6×6 .

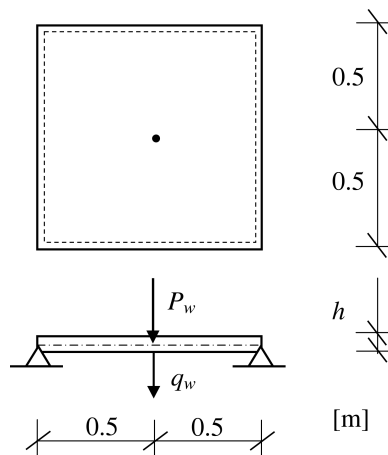


FIG. 2. Plate layout.

6.1. Example 1

The plate from Fig. 2 with thickness $h = 0.05$ m, made from Deltrane 350 rubber, which was introduced in [19], is considered. The following Zener material data are assumed:

$$E_K = 1 \cdot 10^6 \text{ Pa}, \quad E_M = 364 \cdot 10^6 \text{ Pa}, \quad \tau_M = 0.0000052 \text{ s}^\alpha, \quad \alpha = 0.59.$$

The material density is $\rho = 1000 \text{ kg/m}^3$ and the Poisson's ratio $\nu = 0.45$. The temperature data for the Williams-Landel-Ferry formula are taken as for generic rubber from [20]

$$C_1 = 9.23, \quad C_2 = 141.2^\circ\text{C}, \quad T_0 = 20^\circ\text{C}.$$

The plate is loaded by the excitation force (6.2) with the amplitude $P = 50$ N.

The response curves are computed for the given relaxation time in the reference temperature and for three elevated values of service temperature $T = 30, 60, 100^\circ\text{C}$ with the modified relaxation time (2.6). These results are presented in Fig. 3.

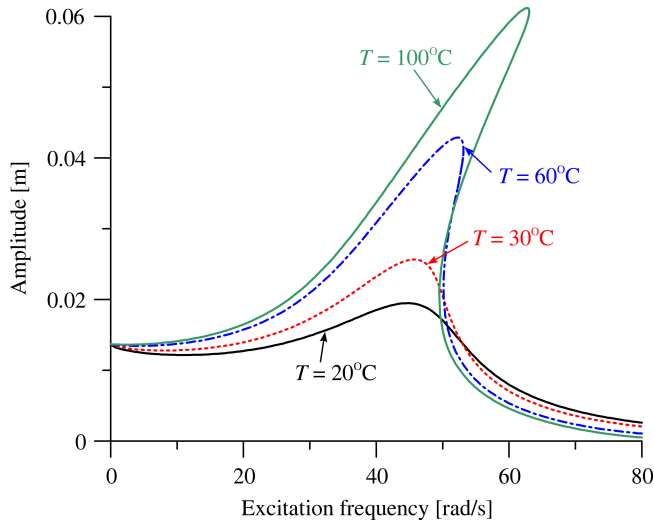


FIG. 3. Response curves for the Deltrane rubber plate – Example 1.

The influence of the temperature change on the dynamic behaviour of the plate is evident. The increase of the temperature, as expected, leads to a decrease of the damping properties of the VE polymer material. This is manifested in the increase of the maximal resonance amplitude of vibration and shift of the resonance frequency corresponding to the maximal vibration amplitude to

higher values. The latter is related to a more emphasised von Kármán non-linear hardening-type behaviour of the plate when the vibration amplitudes approach the magnitude order of the plate thickness. The main characteristics of the resonance behaviour of the plate are summarised in Table 1.

Table 1. Resonance characteristics for the Deltrane rubber plate – Example 1.

T [°C]	20	30	60	100
Max amplitude [m]	0.01948	0.02565	0.04288	0.06117
Resonance frequency [rad/s]	44.8	45.6	52.4	62.8

6.2. Example 2

The plate from Fig. 2 with thickness $h = 0.02$ m, made from epoxy-rubber composite, which was introduced in [27], is considered. The following Zener material data are assumed:

$$E_K = 0.505 \cdot 10^9 \text{ Pa}, \quad E_M = 12.01 \cdot 10^9 \text{ Pa}, \quad \tau_M = 0.00000146 \text{ s}, \quad \alpha = 1.00.$$

The material density is $\rho = 1800 \text{ kg/m}^3$ and the Poisson's ratio $\nu = 0.33$. The temperature data for the Williams-Landel-Ferry formula are taken as for generic epoxy from [23]

$$C_1 = 40.1, \quad C_2 = 51.6^\circ\text{C}, \quad T_0 = 22^\circ\text{C}.$$

The plate is loaded by the excitation force (6.2) with the amplitude $P = 20$ N.

The response curves are computed for the given relaxation time in the reference temperature and for two values of marginally elevated service temperature $T = 24, 26^\circ\text{C}$ with the modified relaxation time (2.6). These results are presented in Fig. 4.

In this case, the influence of even small temperature change is enormous. The resulting decrease of damping in the analysed material is greatly manifested. The change of a few degrees of temperature leads to the 8-times increase of the resonance amplitude and the corresponding shift of the resonance frequency is significant, too. The resonance characteristics are given in Table 2. It should be noted, however, that the results presented here are strongly dependent on the material parameters, which were taken for the generic epoxy. It is therefore evident that there is a great need for good reliable experiments to evaluate the temperature parameters in order to correctly assess the damping properties of VE materials.

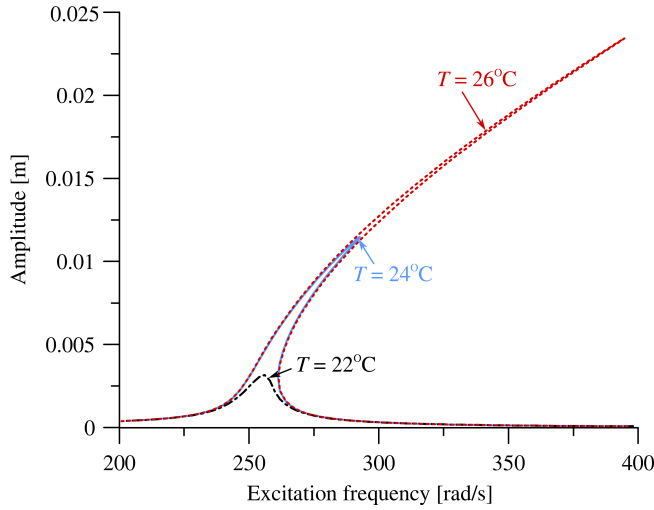


FIG. 4. Response curves for the epoxy-rubber composite plate – Example 2.

Table 2. Resonance characteristics for the epoxy-rubber plate – Example 2.

T [°C]	20	22	24
Max amplitude [m]	0.00317	0.01148	0.02343
Resonance frequency [rad/s]	256	293	395

6.3. Example 3

The plate from Fig. 2 with thickness $h = 0.05$ m, made from nitrile-butadiene rubber (NBR), which was introduced in [13], is considered. The following Zener material data are assumed:

$$E_K = 1.263 \cdot 10^6 \text{ Pa}, \quad E_M = 12.63 \cdot 10^6 \text{ Pa}, \quad \tau_M = 0.016 \text{ s}^\alpha, \quad \alpha = 0.52.$$

The material density is $\rho = 1000 \text{ kg/m}^3$ and the Poisson's ratio $\nu = 0.45$. The temperature data for the Williams-Landel-Ferry formula are taken as for generic rubber from [21]

$$C_1 = 9.23, \quad C_2 = 141.2^\circ\text{C}, \quad T_0 = 20^\circ\text{C}.$$

The plate is loaded by the excitation force (6.2) with the amplitude $P = 50$ N.

The response curves are computed for the given relaxation time in the reference temperature and for five values of elevated service temperature $T = 30, 40, 50, 60, 70^\circ\text{C}$ with the modified relaxation time (2.6). These results are presented in Fig. 5.

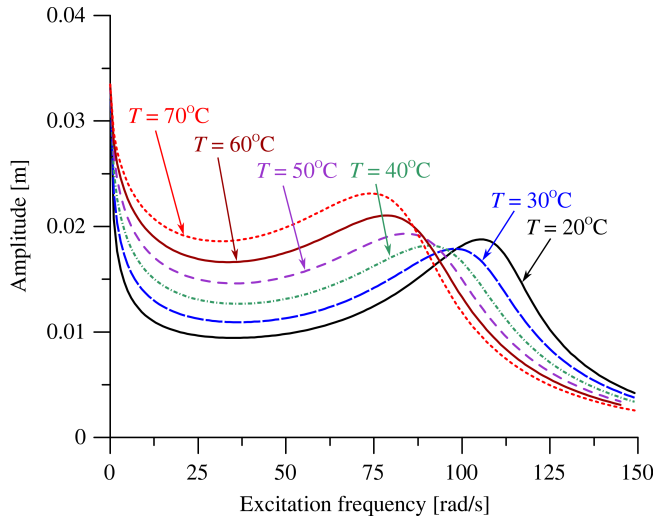


FIG. 5. Response curves for the NBR plate – Example 3.

In this example, which differs from Example 1, where Deltrane rubber was considered, the material is characterised by a significantly higher value of the relaxation time. In such a case, the characteristic behaviour of the Zener model is observed, where the relation between the damping parameter (or relaxation time) and damping effectiveness manifested in the maximal resonance amplitude is not monotonous. Such a phenomenon was already reported in [16, 17]. Here, the increase of the service temperature leads to the decrease of relaxation time, and this results in: first, a decrease of resonance amplitude, and, secondly, after passing the critical value around 30°C , a further increase of resonance amplitude. The change of resonance amplitude is accompanied by the shifting of the resonance frequency. This can be noted in the results presented in Table 3, too.

Table 3. Resonance characteristics for the NBR plate – Example 3.

T [$^{\circ}\text{C}$]	20	30	40	50	60	70
Max amplitude [m]	0.0186	0.0179	0.0182	0.0193	0.0210	0.0231
Resonance frequency [rad/s]	108	98	91	84	79	74

Another curiosity, pertinent to the Zener model, which can be observed in the results in this example, is the fact that the static deflection corresponding to the zero excitation frequency is by far larger than the resonance amplitudes of vibration.

7. CONCLUDING REMARKS

In this paper, the influence of changes of ambient temperature on non-linear, steady-state harmonically forced vibrations of moderately thick viscoelastic plates was analysed. The novelty of the presented analysis is related to: i) the use of the fractional Zener material, ii) the analysis of temperature influence on vibrations of VE plates with the use of time-temperature superposition principle and the Williams-Landel-Ferry formula.

The study of the literature related to these problems indicated that there are great difficulties in finding reliable and complete temperature data for VE material models. There are reports with data for the Zener material model, including its fractional version, but these studies are not accompanied by testing of temperature influence. On the other hand, there are many results presented, where the significant effects of temperature are observed with respect to the relaxation moduli of VE materials. The need for good experiments where materials and structures would be tested under varying temperature conditions is evident.

The use of the classical methods to include the temperature change in the analysis of VE plates indicates that significant qualitative and quantitative effects due to this influence can be observed, including non-monotonous variation of resonance parameters leading to existence of some critical values of material parameters, which correspond to the most or the least effective damping characteristics.

Future work will focused on an extension of the proposed approach to laminated plates with VE layers.

APPENDIX

Strain-displacement relations and the matrices of the differential operators in the amplitude equation (4.15)

$$(A.1) \quad \boldsymbol{\varepsilon}_r = \begin{bmatrix} \frac{\partial}{\partial x} & 0 \\ 0 & \frac{\partial}{\partial y} \\ \frac{\partial}{\partial y} & \frac{\partial}{\partial x} \end{bmatrix} \begin{Bmatrix} \varphi_x \\ \varphi_y \end{Bmatrix} = \mathbf{B}'_r \mathbf{q}_r,$$

$$(A.2) \quad \boldsymbol{\varepsilon}_s = \begin{bmatrix} \frac{\partial}{\partial x} \\ \frac{\partial}{\partial y} \end{bmatrix} \{w^0\} + \begin{bmatrix} 1 & 0 \\ 0 & 1 \end{bmatrix} \begin{Bmatrix} \varphi_x \\ \varphi_y \end{Bmatrix} = \mathbf{B}'_{sw} \mathbf{q}_w + \mathbf{B}'_{sr} \mathbf{q}_r,$$

$$(A.3) \quad \boldsymbol{\varepsilon}_p = \boldsymbol{\varepsilon}_{pl} + \boldsymbol{\varepsilon}_{pn},$$

where

$$(A.4) \quad \boldsymbol{\varepsilon}_{pl} = \begin{bmatrix} \frac{\partial}{\partial x} & 0 \\ 0 & \frac{\partial}{\partial y} \\ \frac{\partial}{\partial y} & \frac{\partial}{\partial x} \end{bmatrix} \begin{Bmatrix} u^0 \\ v^0 \end{Bmatrix} = \mathbf{B}'_r \mathbf{q}_t,$$

$$(A.5) \quad \boldsymbol{\varepsilon}_{pn} = \begin{Bmatrix} \varepsilon_{pn1} \\ \varepsilon_{pn2} \\ \varepsilon_{pn3} \end{Bmatrix},$$

$$(A.6) \quad \begin{aligned} \varepsilon_{pn1} &= \frac{1}{2} \{w^0\}^T \begin{bmatrix} \frac{\partial}{\partial x} \end{bmatrix}^T \begin{bmatrix} \frac{\partial}{\partial x} \end{bmatrix} \{w^0\} = \frac{1}{2} \mathbf{q}_w^T \mathbf{B}'_{w1}{}^T \mathbf{B}'_{w1} \mathbf{q}_w, \\ \varepsilon_{pn2} &= \frac{1}{2} \{w^0\}^T \begin{bmatrix} \frac{\partial}{\partial y} \end{bmatrix}^T \begin{bmatrix} \frac{\partial}{\partial y} \end{bmatrix} \{w^0\} = \frac{1}{2} \mathbf{q}_w^T \mathbf{B}'_{w2}{}^T \mathbf{B}'_{w2} \mathbf{q}_w, \\ \varepsilon_{pn3} &= \frac{1}{2} \left[\{w^0\}^T \begin{bmatrix} \frac{\partial}{\partial x} \end{bmatrix}^T \begin{bmatrix} \frac{\partial}{\partial y} \end{bmatrix} \{w^0\} + \{w^0\}^T \begin{bmatrix} \frac{\partial}{\partial y} \end{bmatrix}^T \begin{bmatrix} \frac{\partial}{\partial x} \end{bmatrix} \{w^0\} \right] \\ &= \frac{1}{2} (\mathbf{q}_w^T \mathbf{B}'_{w1}{}^T \mathbf{B}'_{w2} \mathbf{q}_w + \mathbf{q}_w^T \mathbf{B}'_{w2}{}^T \mathbf{B}'_{w1} \mathbf{q}_w). \end{aligned}$$

REFERENCES

1. ALAVI S.H., EIPAKCHI H., An analytical approach for free vibrations analysis of viscoelastic circular and annular plates using FSDT, *Mechanics of Advanced Materials and Structures*, **27**(3): 250–264, 2018, doi: 10.1080/15376494.2018.1472348.
2. AMABILI M., Nonlinear damping in nonlinear vibrations of rectangular plates: derivation from viscoelasticity and experimental validation, *Journal of the Mechanics and Physics of Solid*, **118**: 275–292, 2018, 10.1016/j.jmps.2018.06.004.
3. AMABILI M., *Nonlinear Mechanics of Shells and Plates: Composite, Soft and Biological Materials*, Cambridge University Press, New York, 2018.
4. AMABILI M., Nonlinear vibrations of viscoelastic rectangular plates, *Journal of Sound and Vibration*, **362**: 142–156, 2010, doi: 10.1016/j.jsv.2015.09.035.
5. ATANACKOVIC T.M., A modified Zener model of a viscoelastic body, *Continuum Mechanics and Thermodynamics*, **14**(2): 137–148, 2002, doi: 10.1007/s001610100056.
6. BAGLEY R.L., TORVIK P.J., A theoretical basis for the application of fractional calculus to viscoelasticity, *Journal of Rheology*, **27**(3): 201–210, 1983, doi: 10.1122/1.549724.

7. BAGLEY R.L., TORVIK P.J., On the fractional calculus model of viscoelastic behaviour, *Journal of Rheology*, **30**(1): 133–155, 1986, doi: 10.1122/1.549887.
8. BRINSON H.F., BRINSON L.C., *Polymer Engineering Science and Viscoelasticity. An Introduction*, Springer, New York, 2008.
9. ELDRED L.B., BAKER W.P., PALAZOTTO A.N., Kelvin-Voigt versus fractional derivative model as constitutive relations for viscoelastic materials, *AIAA Journal*, **33**(3): 547–550, 1995, doi: 10.2514/3.12471.
10. ESHMATOV B.K., Nonlinear vibrations and dynamic stability of viscoelastic orthotropic rectangular plates, *Journal of Sound and Vibration*, **300**(3–5): 709–726, 2007, doi: 10.1016/j.jsv.2006.08.024.
11. GOPALAN V., SUTHENTHIRAVEERAPPA V., PRAGASAM V., Experimental and numerical investigation on the dynamic characteristics of thick laminated plant fiber-reinforced polymer composite plates, *Archive of Applied Mechanics*, **89**(2): 363–384, 2019, doi: 10.1007/s00419-018-1473-8.
12. LEWANDOWSKI R., Influence of temperature on the dynamic characteristics of structures with viscoelastic dampers, *Journal of Structural Engineering*, **145**(2): 04018245, 2019, doi: 10.1061/(ASCE)ST.1943-541X.0002238.
13. LEWANDOWSKI R., PRZYCHODZKI M., Approximate method for temperature-dependent characteristics of structures with viscoelastic dampers, *Archive of Applied Mechanics*, **88**(10): 1695–1711, 2018, doi: 10.1007/s00419-018-1394-6.
14. LI H., GOMEZ D., DYKE S.J., XU Z., Fractional differential equation bearing models for base-isolated buildings: framework development, *Journal of Structural Engineering*, **146**(2): 04019197, 2020, doi: 10.1061/(ASCE)ST.1943-541X.0002508.
15. LIJUN Y., XUELIANG J., The natural transverse vibration of rectangular thick plates with viscoelastic on viscoelastic foundation, *Electronic Journal of Geotechnical Engineering*, **19**: 3173–3179, 2014.
16. LITEWKA P., LEWANDOWSKI R., Nonlinear harmonically excited vibrations of plates with Zener material, *Nonlinear Dynamics*, **89**(1): 691–712, 2017, doi: 10.1007/s11071-017-3480-7.
17. LITEWKA P., LEWANDOWSKI R., Steady-state non-linear vibrations of plates using Zener material with fractional derivative, *Computational Mechanics*, **60**(2): 333–354, 2017, doi: 10.1007/s00466-017-1408-1.
18. MAKRIS N., CONSTANTINOUC M.C., Fractional-derivative Maxwell model for viscous dampers, *Journal of Structural Engineering*, **117**(9): 2708–2724, 1991, doi: 10.1061/(ASCE)0733-9445(1991)117:9(2708).
19. MORIN B., LEGAY A., DEÛ J-F., Reduced order models for dynamic behavior of elastomer damping devices, *Finite Elements in Analysis and Design*, **143**: 66–75, 2018, doi: 10.1016/j.finel.2018.02.001.
20. PERMOON M.C., HADDADPOUR H., JAVADI M., Nonlinear vibration of fractional viscoelastic plate: primary, subharmonic, and superharmonic response, *International Journal of Non-Linear Mechanics*, **99**: 154–164, 2018, doi: 10.1016/j.ijnonlinmec.2017.11.010.
21. PIRK R., ROULEAU L., DESMET W., PLUYMERS B., Validating the modeling of sandwich structures with constrained layer damping using fractional derivative models, *Journal of*

- the Brazilian Society of Mechanical Sciences and Engineering*, **38**(7): 1959–1972, 2016, doi: 10.1007/s40430-016-0533-7.
22. PODLUBNY I., *Fractional Differential Equations*, Academic Press, 1998.
 23. SALEHI M., AGHAEI H., Dynamic relaxation large deflection analysis of non-axisymmetric circular viscoelastic plates, *Computers and Structures*, **83**(23–24): 1878–1890, 2005, doi: 10.1016/j.compstruc.2005.02.023.
 24. SHAW M.T., *Introduction to Polymer Rheology*, Wiley, New Jersey, 2012.
 25. TOUATI D., CEDERBAUM G., Dynamic stability of nonlinear viscoelastic plates, *International Journal of Solids and Structures*, **31**(17): 2367–2376, 1994, doi: 10.1016/0020-7683(94)90157-0.
 26. TROGDON S.A., Small amplitude vibration of viscoelastic plates, *Acta Mechanica*, **53**(3): 233–243, 1984, doi: 10.1007/BF01177953.
 27. XU X., GAO S., ZHANG D., NIU S., JIN L., OU Z., Mechanical behavior of liquid nitrile rubber-modified epoxy resin: experiments, constitutive model and application, *International Journal of Mechanical Sciences*, **151**: 46–60, 2019, doi: 10.1016/j.ijmecsci.2018.11.003.

Received October 15, 2019; accepted version February 3, 2020.

Published on Creative Common licence CC BY-SA 4.0

